

Electronic Supplementary Information (ESI)

Postsynthesis of MSE-type titanosilicate by interzeolite transformation for selective anisole hydroxylation

Rusi Peng,^a Huang Pan,^a Xintong Li,^a Shaoqing Jin,^b Zhendong Wang,^b Jingang Jiang,^a
Weimin Yang,^b Hao Xu*^{a,c} and Peng Wu*^{a,c}

^a Shanghai Key Laboratory of Green Chemistry and Chemical Processes, School of Chemistry and Molecular Engineering, East China Normal University, North Zhongshan Road 3663, Shanghai, 200062, China

^b State Key Laboratory of Green Chemical Engineering and Industrial Catalysis, Sinopec Shanghai Research Institute of Petrochemical Technology, Shanghai, 201208, China

^c Institute of Eco-Chongming, Shanghai, 202162, China

Corresponding authors: pwu@chem.ecnu.edu.cn (P. WU); hxu@chem.ecnu.edu.cn (H. XU)

Table S1 Summary for the synthesis of MSE-type aluminosilicates by interzeolite conversion method from siliceous Beta zeolite under different crystallization conditions ^a

No.	Gel composition ^b						Product		
	Si/Al	(K ⁺ + Na ⁺)/Si	K ⁺ /Na ⁺	OSDA/Si	seed/Si	H ₂ O/Si	phase	Si/Al ^c	yield ^d (%)
1	12	0.5	0	0.3	0.2	15	*BEA with a trace of MSE	-	-
2	12	0.5	0.33	0.3	0.2	15	MSE + *BEA	-	-
3	12	0.5	1	0.3	0.2	15	MSE with a trace of *BEA	-	-
4	12	0.5	3	0.3	0.2	15	MSE	8.2	68.4
5	12	0.5	∞	0.3	0.2	15	MSE	8.5	74.2
6	12	0.375	∞	0.3	0.2	15	MSE with a trace of *BEA	-	-
7	12	0.4	∞	0.3	0.2	15	MSE	8.0	70.8
8	12	0.6	∞	0.3	0.2	15	MSE with a trace of MFI	-	-
9	60	0.5	∞	0.3	0.2	15	KHSi ₂ O ₅	-	-
10	15	0.5	∞	0.3	0.2	15	MSE + KHSi ₂ O ₅	-	-
11	11	0.5	∞	0.3	0.2	15	MSE	8.1	76.0
12	10	0.5	∞	0.3	0.2	15	MSE	8.3	83.7
13	9.2	0.5	∞	0.3	0.2	15	MSE with a trace of *BEA	-	-
14	10	0.5	∞	0.3	0.2	15	MSE	8.5	84.7
15	10	0.5	∞	0.25	0.2	15	MSE	8.2	81.3
16	10	0.5	∞	0.22	0.2	15	MSE	8.6	84.9
17	10	0.5	∞	0.2	0.2	15	MSE with a trace of *BEA	-	-
18	10	0.5	∞	0.22	0.17	15	MSE	8.8	86.9
19	10	0.5	∞	0.22	0.15	15	MSE with a trace of *BEA	-	-
20	10	0.5	∞	0.22	0.17	10	MSE	8.5	84.1
21	10	0.5	∞	0.22	0.17	5	MSE	8.9	88.3
22 ^e	10	0.5	∞	0.22	0.17	15	MSE	8.4	83.2
23 ^f	10	0.5	∞	0.22	0.17	15	MSE	7.9	75.9

^a The gels were treated at 413 K for 1 h before adding seed and AlCl₃, and then crystallized at 433 K for 23 h.

^b Si/Al ratio corresponding to the molar ratio of total Si to the total Al amount in both parent zeolite and seed.

^c Given by ICP analysis.

$$^d \text{ Solid yield} = \frac{m(\text{calcined product})}{m(\text{siliceous Beta}) + m(\text{Al}_2\text{O}_3) + m(\text{seed})} \times 100\%$$

^e Calcined siliceous BEA synthesized following reference [1] as the silica source.

^f Calcined MSE-*trans* (sample No. 18) as the seed.

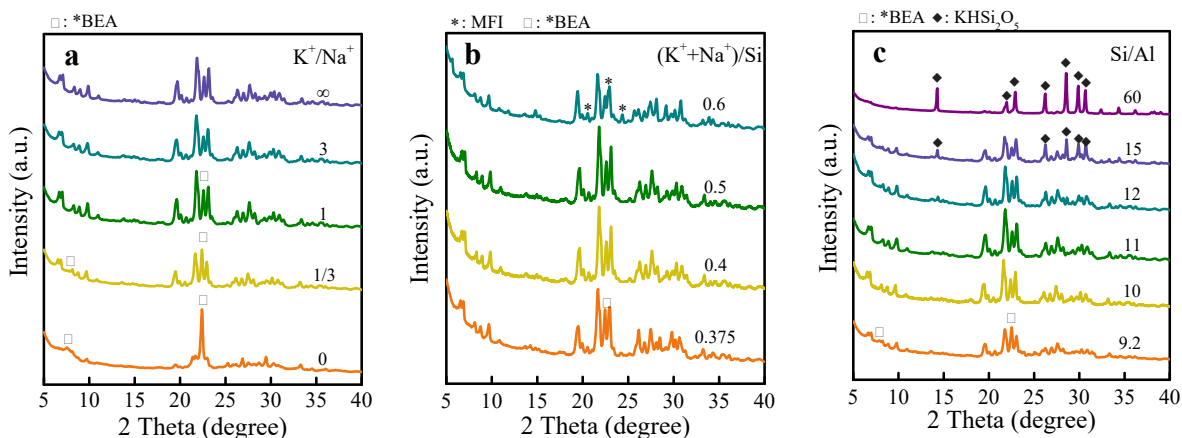


Fig. S1 XRD patterns of the products synthesized with different K^+/Na^+ molar ratio (a), $(K^++Na^+)/Si$ molar ratio (b) and Si/Al molar ratio (c). Crystallization conditions: TEAOH/Si = 0.25; Si/Al = 11 (a, b); $K^+/Na^+ = \infty$ (b, c); $(K^++Na^+)/Si = 0.5$ (a, c); $H_2O/Si = 15$; other conditions, see Table S1. Si/Al ratio was defined as the molar ratio of total Si to the total Al amount in both parent zeolite and seed.

As summarized in Table S1 and Fig. S1, the synthesis of pure-phase MSE-trans zeolite highly depended on the chemical compositions of the gel mixtures, especially the Si/Al ratio and K^+ content. With higher K^+/Na^+ ratios, *BEA phase was inhibited and the MSE phase was the main product (Table S1, Nos. 1-5 and Fig. S1a).

Moreover, the $(K^++Na^+)/Si$ ratio of 0.375 led to the impurity of Beta phase, and an incremental $(K^++Na^+)/Si$ ratio up to 0.6 resulted in a minor amount of MFI phase (Table S1, Nos. 6-8 and Fig. S1b). With the $(K^++Na^+)/Si$ ratio fixed at 0.5, pure MSE-trans zeolite was produced with the Si/Al ratio varied in the range of 10 - 12 (Table S1, Nos. 9-13 and Fig. S1c). Under the above optimized crystallization conditions, the critical value of TEAOH/Si and seed/Si for producing pure-phase MSE-type samples could be reduced to 0.22 and 0.17, respectively (Table S1, Nos. 14-19). Notably, the yield of MSE-trans reached up to 88.3% by reducing the H_2O/Si ratio from 15 to 5 (Table S1, Nos. 20 and 21), considerably higher than that of MSE-type zeolite synthesized from the system involving TEAOH, $Al(OH)_3$ and fumed silica (yield: 54.0%) [2]. In addition, the siliceous Beta zeolites synthesized by different methods (dealumination and direct hydrothermal synthesis) showed no effect on interzeolite transformation (Table S1, No. 18 and No. 22). The calcined MSE-trans material was further employed as seed to produce the "second-generation" MSE-trans successfully (Table S1, No. 23). The results above revealed that parent zeolite and the seeds with the same CBUs or

crystalline structure as the product as well as the organic quaternary ammonium cations with structure-directing ability are indispensable to realize this interzeolite transformation.

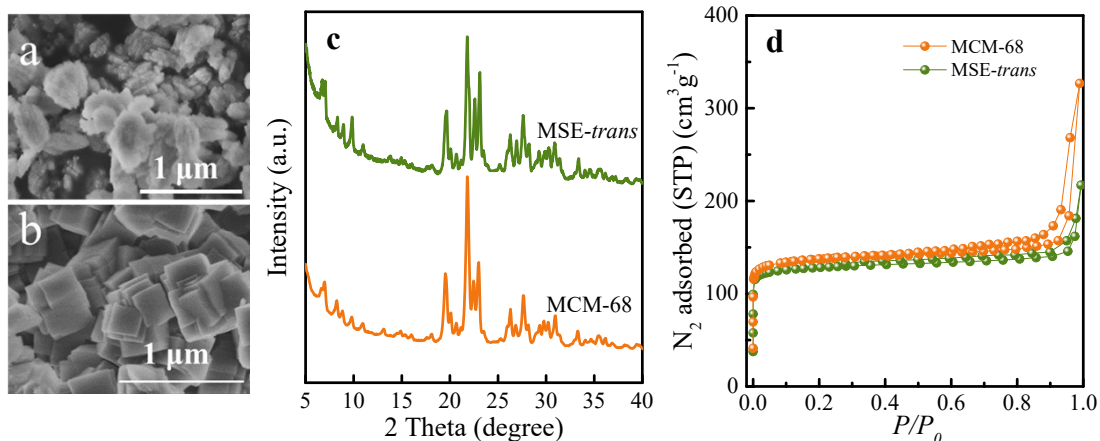


Fig. S2 SEM images of conventional MCM-68 (a) and MSE-*trans* (b), and XRD patterns (c) and N₂ adsorption-desorption isotherms (d) of MSE-type aluminosilicates synthesized by different methods.

The crystals of the conventional MCM-68 synthesized using *N, N, N', N'*-tetraethylbicyclo [2.2.2] oct-7-ene-2, 3: 5, 6- dipyrrolidinium diiodide (TEBOP²⁺(I)₂) as OSDA was composed of 50 - 100 nm particles, while the MSE-*trans* zeolite consisted of the aggregates of rectangle nano-particles with a larger size of 200 - 500 nm (Fig. S2, a and b). The two samples showed the XRD diffraction peaks assigned to the MSE topology (Fig. S2c), with high crystallinity. They exhibited type I N₂ sorption isotherms, characteristic of typical microporous materials. They also possessed the intracrystal mesoporosity, revealed by increased multilayer adsorption at $P/P_0 > 0.85$ (Fig. S2d).

Table S2 Physicochemical properties of various MSE-type aluminosilicates

Sample	Si/Al		SSA (cm ² g ⁻¹)			Pore volume (cm ³ g ⁻¹)		
	gel	product ^a	S _{total} ^b	S _{micro}	S _{ext} ^c	V _{total} ^d	V _{micro} ^c	V _{meso} ^e
MCM-68	12	10	484	392	92	0.43	0.19	0.24
MSE-trans	10	8.9	438	373	65	0.27	0.17	0.10

^a Determined by ICP.

^b Specific surface area (SSA) calculated by BET method.

^c Calculated by *t*-plot method.

^d Determined by the adsorption amount at P/P₀ = 0.99.

^e V_{meso} = V_{total} - V_{micro}.

The Al content in MSE-trans (with a lower Si/Al ratio) was higher than that in conventional MCM-68. Furthermore, MSE-trans exhibited slightly lower specific area and mesopore volume than MCM-68, probably because the former had a larger crystal size.

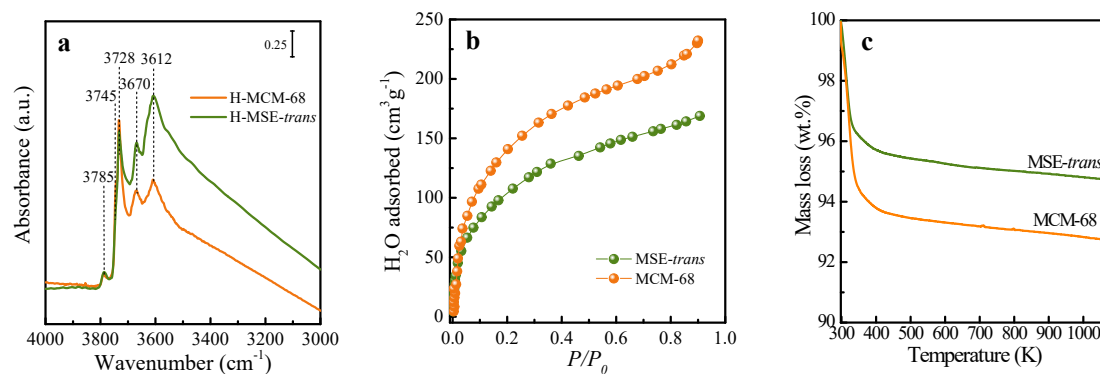


Fig. S3 IR spectra in the hydroxyl stretching region (a), H₂O adsorption curves (b) and thermogravimetric curves after saturated with water vapor over aqueous NH₄Cl solution overnight (c) for two kinds of MSE-type aluminosilicates.

Compared with conventional MCM-68, the MSE-trans zeolite showed more obvious bands attributed to Si-OH-Al (3612 cm⁻¹) and extra-framework Al-OH (3670 cm⁻¹) (Fig. S3a), mostly due to the higher Al content in MSE-trans (Table S2). Furthermore, the intensity of bands assigned to external Si-OH (3745 cm⁻¹) in two MSE samples was similar, but MSE-trans sample showed a slightly weaker band assigned to internal Si-OH (3728 cm⁻¹) (Fig. S3a). Thus, MSE-trans was more hydrophobic than MCM-68 (Fig. S3, b and c).

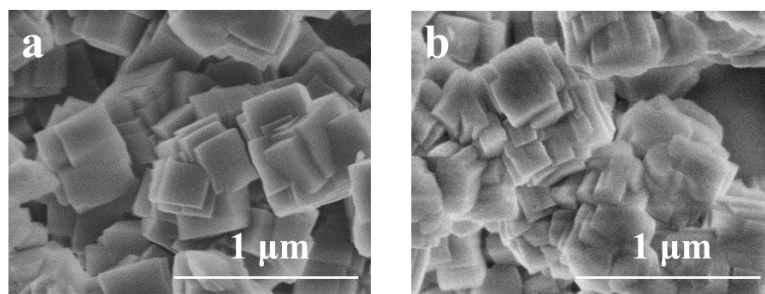


Fig. S4 SEM images of MSE-*trans* (a) and Ti-MSE-*trans* (b).

The dealumination treatment and further Ti insertion barely altered the crystal morphology.

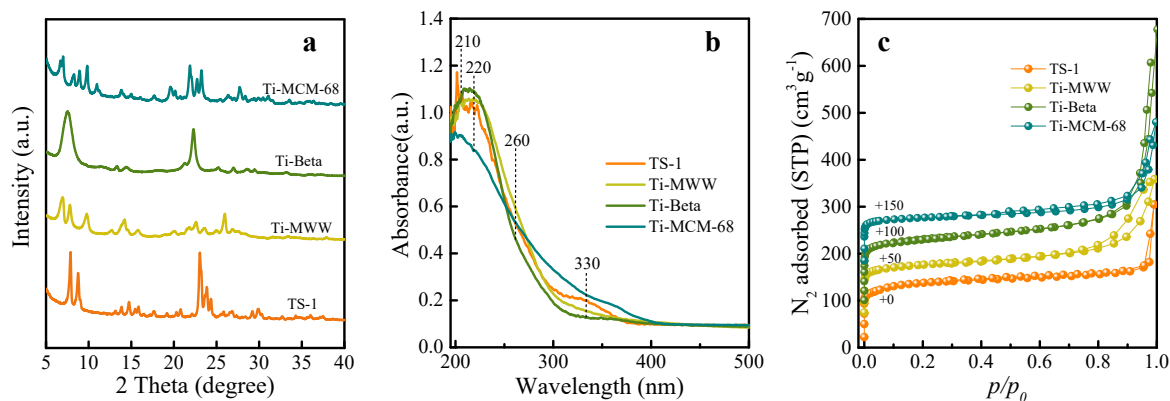


Fig. S5 XRD patterns (a), UV-vis spectra (b) and N₂ adsorption and desorption isotherms (c) of various titanasilicates.

The four titanasilicates (TS-1, Ti-MWW, Ti-Beta and Ti-MCM-68) for control experiment were all highly crystalline materials with typical microporous characteristic (Fig. S5, a and c). Their Ti species were mainly tetrahedrally coordinated in the frameworks, while minor extra-framework Ti species (260 nm) and anatase (330 nm) co-existed in TS-1 and Ti-MCM-68 as shown by UV-vis spectra (Fig. S5b).

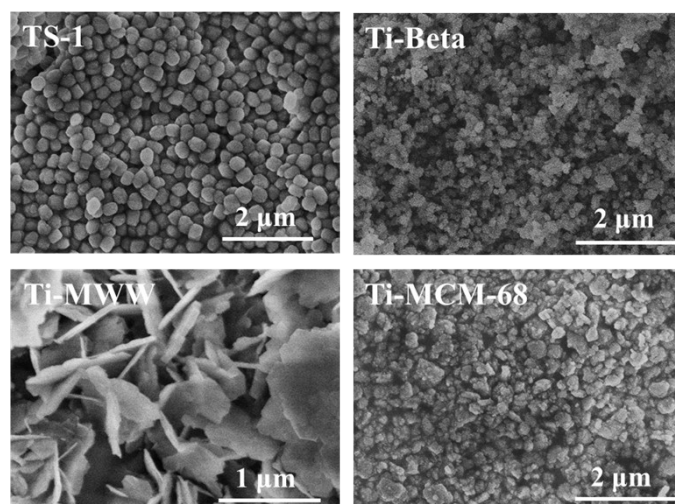


Fig. S6 SEM images of various reference titanossilicates.

TS-1 possessed nanosized sphere crystals with a size of ~200 nm. Ti-Beta and Ti-MCM-68 were composed of nanosized crystalline particles with a particle size in the range of 50 - 100 nm. Ti-MWW showed a platelet-like morphology with a thickness of ~100 nm.

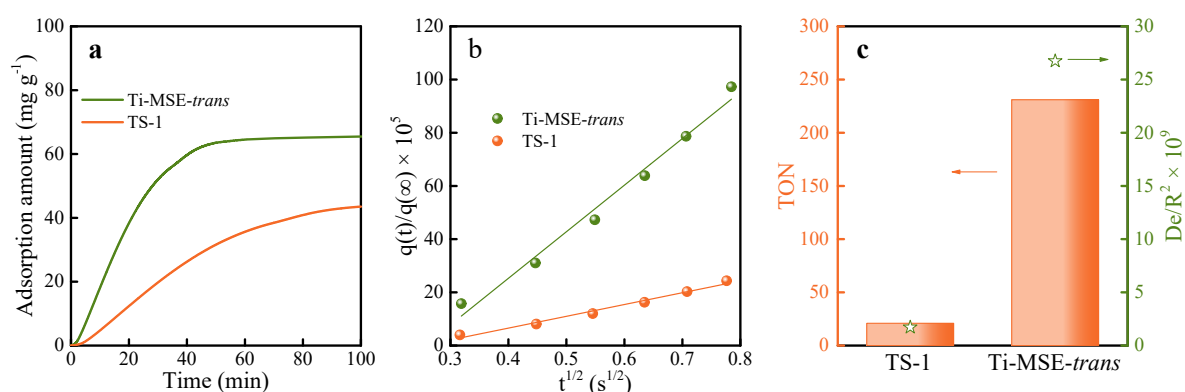


Fig. S7 Comparison between Ti-MSE-*trans* and TS-1 for the adsorption profiles of gaseous anisole molecules (a) and the dependence of $q(t)/q(\infty)$ ratio with $t^{1/2}$ (b). Correlation of TON with De/R^2 value (c).

According to the adsorption curves (Fig. S7a), Ti-MSE-*trans* exhibited more saturation adsorption amount of anisole (65.5 mg g⁻¹) than TS-1 (44.2 mg g⁻¹). Following the Fick's second law, the plot of $q(t)/q(\infty)$ ratio versus $t^{1/2}$ is linear in the initial adsorption region (within 1 min) (Fig. S7b), and thus the diffusion coefficient D_e/R^2 could be estimated from the slope [3,4]. It could be observed that Ti-MSE-*trans* exhibited a much larger diffusion coefficient than TS-1 (Fig. S7c), due to the wider channel system (Table S3). Moreover, Ti-MSE-*trans* also exhibited a much higher turnover number (TON) than TS-1 in anisole hydroxylation (Fig. S7c). It could be deduced that the weaker diffusion limitation and steric hindrance in Ti-MSE-*trans* with large-pore channels might dominantly contribute to the superior catalytic performance compared to medium-pore TS-1. In addition, Ti-MSE-*trans* had a higher saturated adsorption amount of anisole than TS-1, which should be also beneficial to the hydroxylation of anisole.

Table S3 The pore size and dimension of catalysts. ^a

Code	MSE	MFI
Pore size (Å)	[001] 6.4×6.8	
	↔	[100] 5.1×5.5
	[100] 5.2×5.8	↔
	↔	[010] 5.3×5.6
	[110] 5.2×5.2	
Pore window and channel dimension	$12 \times 10 \times 10$	10×10

^a The data are obtained from the International Zeolite Association (www.iza-structure.org/databases).

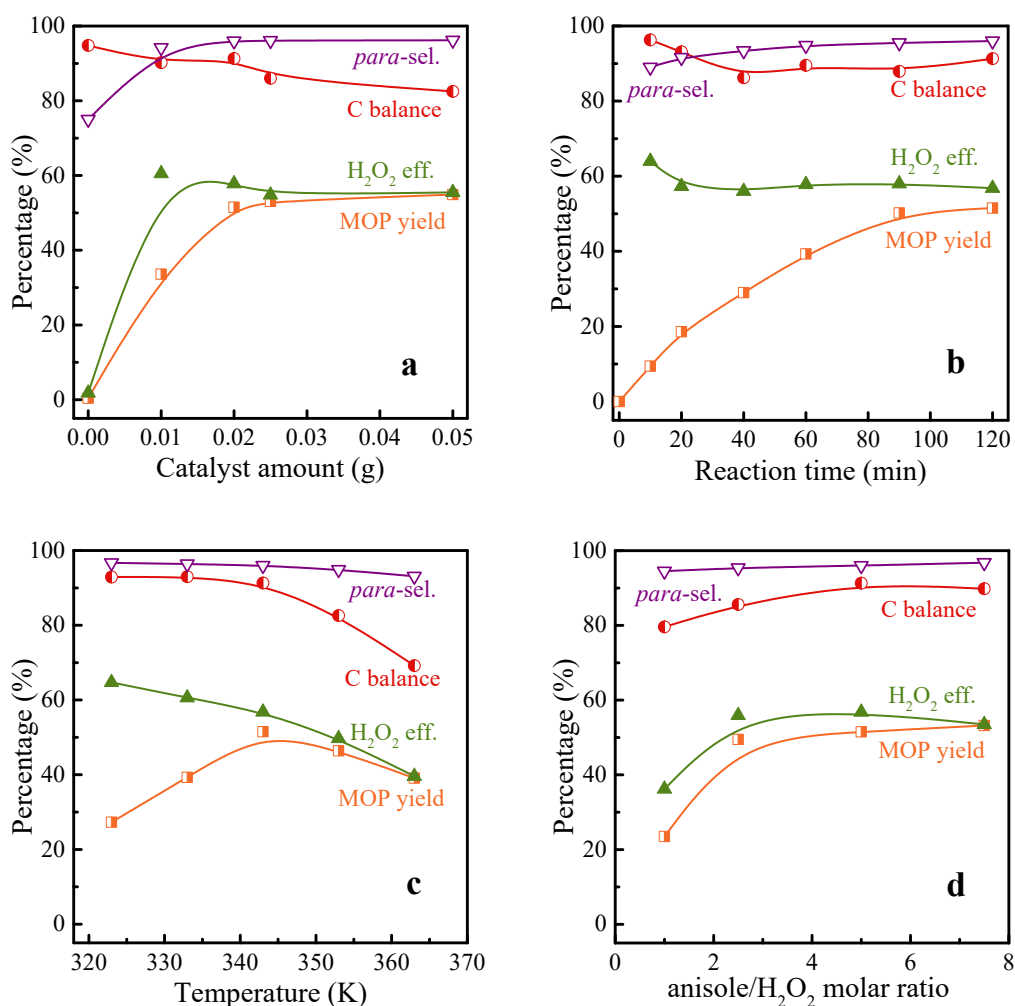


Fig. S8 Effect of catalyst amount (a), reaction time (b), temperature (c) and anisole/H₂O₂ molar ratio (d) on anisole hydroxylation over Ti-MSE-*trans*. Reaction conditions: Ti-MSE-*trans*, 0.02 g (B, C, D); MeOH, 4 g; anisole, 20 mmol (A, B, C); H₂O₂ (33.0 wt.%), 4 mmol; temperature, 343 K (A, B, D); time, 2 h (A, C, D).

As shown in Fig. S8a, the MOP yield and *para*-selectivity notably increased with the increase of catalyst amount up to 0.025 g and then almost leveled off. Nevertheless, with the increase of catalyst amount, H₂O₂ efficiency and carbon balance exhibited slight decrease from 60.5% to 55.5% and 90.2% to 82.5%, respectively. This indicated that excess catalyst promoted the noneffective consumption of H₂O₂ and formation of undetectable tar.

The MOP yield increased monotonically with the reaction time, up to 51.5% at 120 min, and a slightly increased *para*-selectivity was also observed with the increase of time (Fig. S8b). Moreover, H₂O₂ utilization efficiency decreased from 64% to 57.3% at initial stage, and nearly leveled off with further prolonging time, indicating that the non-productive decomposition of H₂O₂ might be more intense at the preliminary stage of reaction.

With the temperature elevated (Fig. S8c), the para-selectivity exhibited a slight decrease. However, the MOP yield exhibited a volcano-shaped change and reached the maximum of 51.5% at 343 K. Furthermore, H₂O₂ utilization efficiency and carbon balance significantly declined with the increase of reaction temperature. It could be concluded that higher reaction temperature not only promoted the non-productive decomposition of H₂O₂, but also intensified the over oxidation and formation of undetectable tar, which has also been previously reported in phenol hydroxylation [5].

Moreover, the effect of anisole/H₂O₂ ratio was also investigated by adjusting the amount of anisole while keeping H₂O₂ amount constant (Fig. S8d). Upon increasing the anisole/H₂O₂ molar ratio, the MOP yield and H₂O₂ utilization efficiency increased gradually and reached a plateau at anisole/H₂O₂ ratios of 5 - 10. The para-selectivity and carbon balance increased from 94.5% to 96.8% and from 79.6% to 91.3%, respectively, with increasing the anisole/H₂O₂ ratio from 1 to 10. It suggested that the side reactions and self-decomposition of H₂O₂ were more significant at lower anisole/H₂O₂ molar ratios.

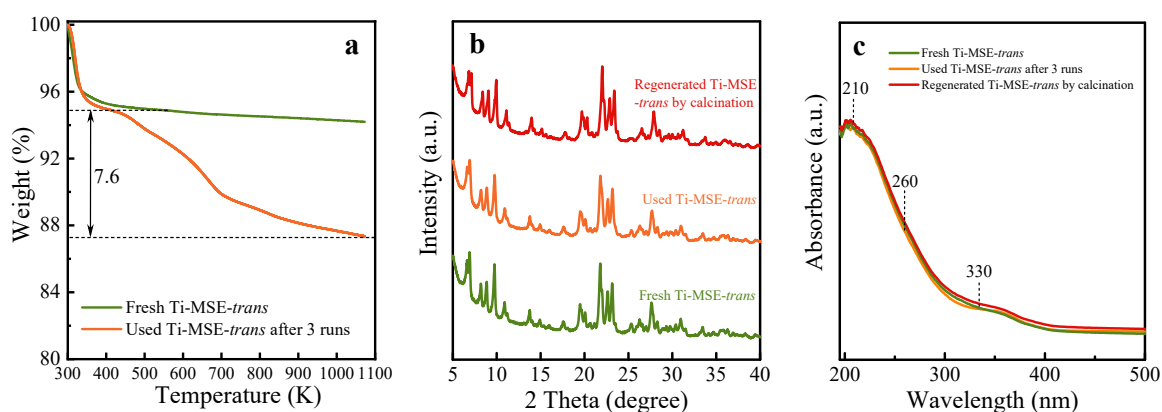
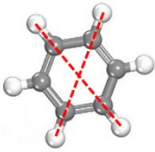
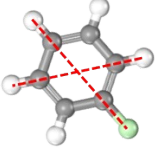
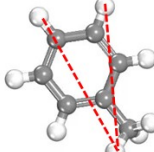
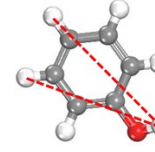
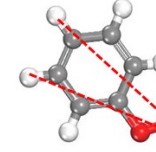


Fig. S9 The comparison of TG curves (a) of the fresh and used catalyst, XRD patterns (b) and UV-vis spectra (c) of fresh, used and regenerated Ti-MSE-*trans*.

After the third run in anisole hydroxylation, there was about 7.6 wt.% organic substrates in the used catalyst (Fig. S9a). The used and regenerated Ti-MSE-*trans* possessed the intact crystallinity and almost unaltered coordination of Ti sites in comparison to the fresh one (Fig. S9b, S9c), indicating that the deposition of organic substrates was mainly responsible for the deactivation in anisole hydroxylation.

Table S4 The kinetic molecular sizes of the substrates ^a

	Benzene	Chlorobenzene	Toluene	Phenol	Anisole
Substrate					
Size (Å)	5.4 × 5.4	5.7 × 5.4	6.2 × 5.8	6.2 × 5.8	7.5 × 7.0

^a The data were calculated with the software Materials Studio.

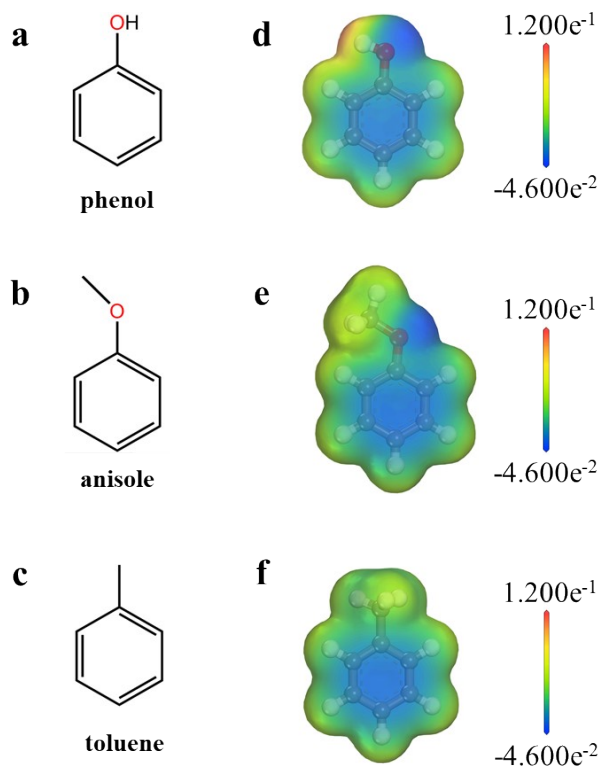


Fig. S10 Molecular structures of three aromatics in this work: (a) phenol, (b) anisole and (c) toluene. The corresponding electrostatic potentials (ESP) (d, e and f) mapped onto their electron density surface.

More negative electrostatic potentials (ESP) were observed in phenol and anisole both with O in substituent groups than toluene, indicating that the O atoms bonded to benzene rings would be more prone to interact with the hydroxyls of zeolite framework in the catalytic reactions.

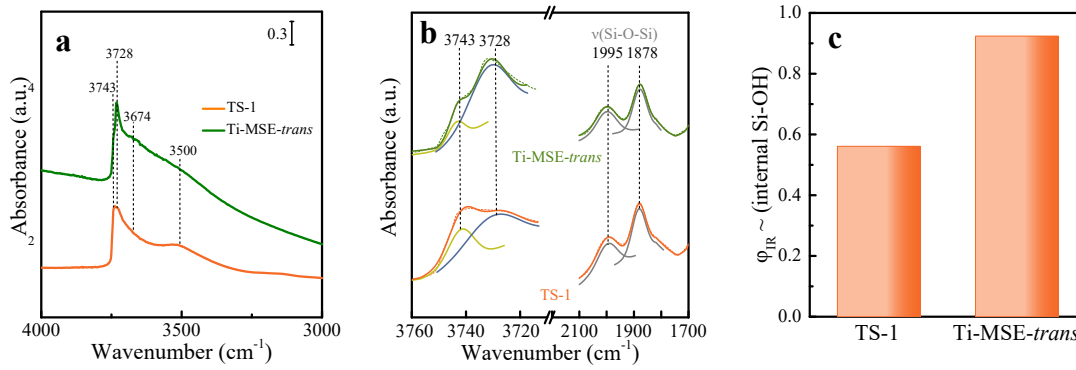
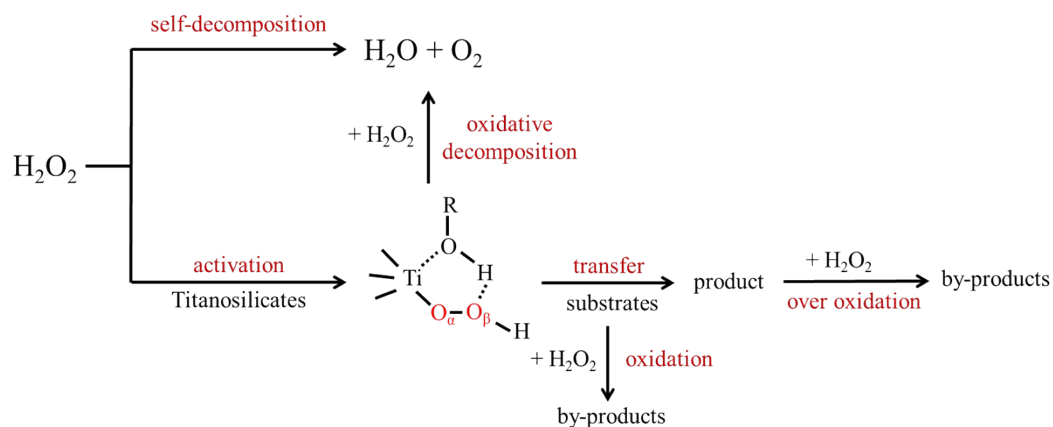


Fig. S11 IR spectra in the hydroxyl stretching vibration region (a) and corresponding deconvolution analysis of IR spectra (b) and φ_{IR} value (c) of TS-1 and Ti-MSE-*trans*.

The relative densities of internal Si-OH groups for TS-1 and Ti-MSE-*trans* catalysts could be quantified by taking the area of $\nu(O-H)$ of internal Si-OH with respect to the area of $\nu(Si-O-Si)$ bands [6]:

$$\varphi_{IR} = \frac{A_{\nu(Si-OH)}}{A_{\nu(Si-O-Si)}} \quad (1)$$

As shown in Fig. S11a and b, the band at 3728 cm^{-1} was more intense for Ti-MSE-*trans* compared to TS-1. And the semi-quantitatively calculated φ_{IR} value of internal Si-OH in Ti-MSE-*trans* (0.924) was more than that in TS-1 (0.561) (Fig. S11c). These indicated that the existence of more internal Si-OH groups in Ti-MSE-*trans*.



Scheme S1 The reaction pathways of H_2O_2 during liquid-phase oxidation catalyzed by titanosilicates.

As illustrated in Scheme S1, the behaviors and pathways of H_2O_2 conversion were relatively complicated, involving the activation over Ti sites to form the TiOOH intermediate species and then the transfer of active "O" to reactant molecules. In addition, the self-decomposition of H_2O_2 , oxidative decomposition of H_2O_2 with TiOOH species were unavoidable. Moreover, the direct oxidation of reactants to by-products and over oxidation of products also led to non-productive consumption of H_2O_2 .

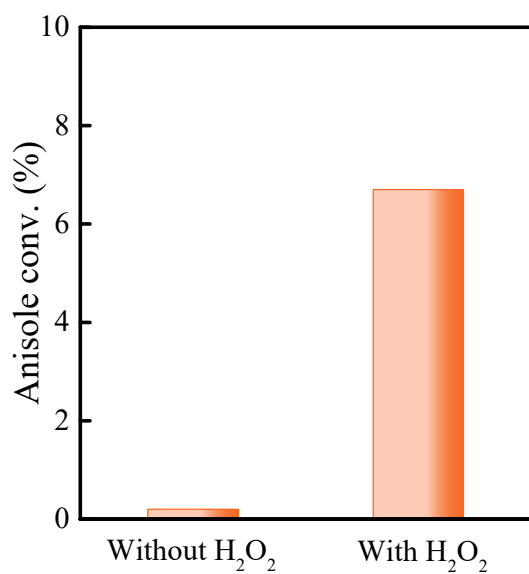


Fig. S12 The conversion of anisole without Ti-MSE-*trans* under different condition. Reaction condition: MeOH, 4 g; anisole, 20 mmol; H₂O₂ (33.0 wt.%), 4 mmol (if added); temperature, 343 K; time, 1 h.

Without the catalyst and H₂O₂, anisole barely converted. Non-catalytic oxidation of anisole with H₂O₂ addition occurred at a limited level, which dominantly produced phenol and traces of diphenols, methoxyphenols, etc.

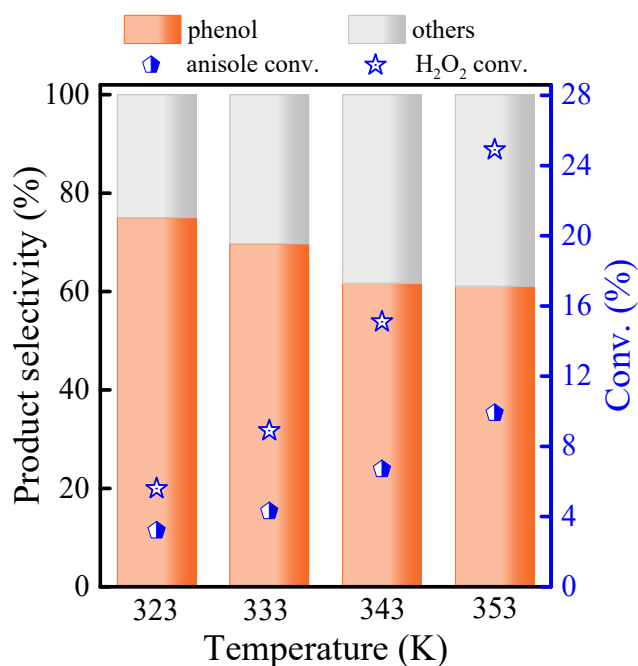


Fig. S13 The conversion of anisole without the presence of Ti-MSE-*trans* at different temperatures. Reaction condition: MeOH, 4 g; anisole, 20 mmol; H₂O₂ (33.0 wt.%), 4 mmol; time, 1 h.

According to the product distribution, phenol was the dominant product in the anisole oxidation system without Ti-MSE-*trans*, and the by-products included diphenols, traces of methoxyphenols and various aromatics hardly distinguished via GC analysis. At 343 K, the phenol yield was ~4.1% in 1 h (Fig. S13) while the MOP yield was only 0.4% formed after 2 h (Fig. S8a) in the catalyst-free system, suggesting the reaction selectively occurred in favor of the oxidative demethylation rather than the hydroxylation of anisole. In addition, with the temperature was raised, the conversion of anisole and H₂O₂ both increased while the proportion of phenol in products declined. This indicated that higher temperature possibly intensified the oxidative demethylation of anisole and further phenol oxidation. Furthermore, the H₂O₂ utilization efficiency in anisole conversion decreased from 57.0% to 39.7% with the temperature elevated from 323 K to 353 K. It might be caused by the intensified self-decomposition and over oxidation at higher temperature.

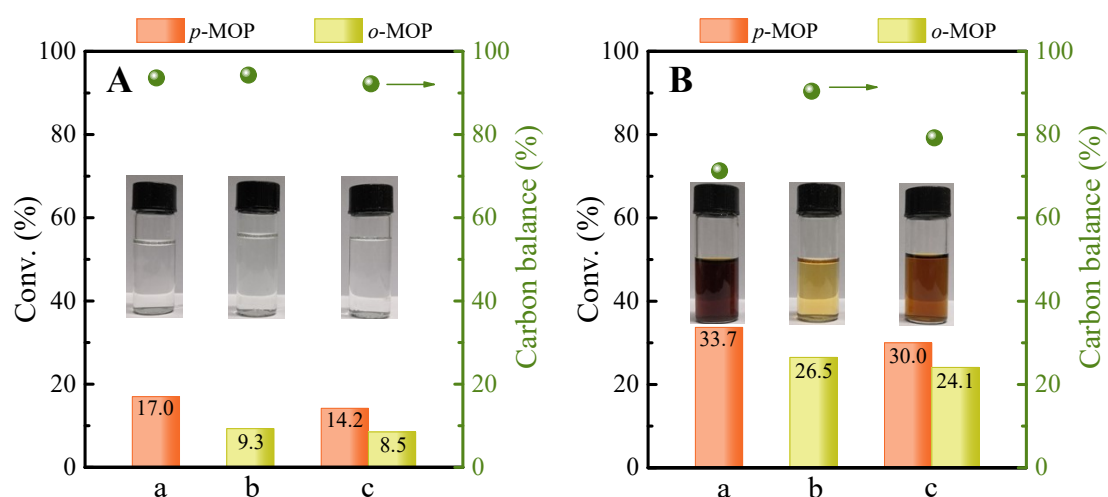


Fig. S14 The conversion of *p*-MOP and/or *o*-MOP without (A) and with (B) the presence of Ti-MSE-*trans*. Reaction conditions: Ti-MSE-*trans*, 0.02 g (if added); MeOH, 4.0 g; H₂O₂ (33.0 wt.%), 4 mmol; *p*-MOP, 2 mmol (a); *o*-MOP, 2 mmol (b), *p*-MOP, 1 mmol and *o*-MOP, 1 mmol (c); temperature, 333 K; time, 0.5 h. The insets show the pictures of reaction solution.

Fig.S14 compares the oxidation of MOP isomers with H₂O₂ in the absence or presence of Ti-MSE-*tran* catalyst. In the catalyst-free system (Fig. S14A), higher conversion of *p*-MOP than *o*-MOP was observed, irrespective of the reaction system containing single isomer or two isomers. The carbon balance values in all three tests were above 90%, and the corresponding reaction filtrates were clear and colorless. When Ti-MSE-*trans* was added, the conversions of MOP isomers were all enhanced compared to the catalyst-free system (Fig. S14B). Nevertheless, similar trends could be observed that *p*-MOP exhibited higher conversion than *o*-MOP, and the values of $\text{conv.}_p/\text{conv.}_o$ was comparable for the single isomer and two isomers system. This phenomenon indicated that the *para*-isomer was more prone to be over oxidized than the *ortho*-isomer in the practical anisole hydroxylation reaction, which would decrease the apparent *para*-selectivity. In addition, the distinct darkening reaction solution and decreased carbon balance values in catalyst-containing system indicated the tar formation through over oxidation catalyzed by Ti-MSE-*trans*, and the over oxidation of *p*-MOP isomer took major responsibility for tar formation.

Reference:

- [1] C. T. Brigden and C. D. Williams, *Microporous and Mesoporous Mater.*, 2007, **100**, 118-127.
- [2] S. Sogukkanli, K. Iyoki, S. P. Elangovan, K. Itabashi, M. Takano, Z. Liu, S. Inagaki, T. Wakihara, Y. Kubota and T. Okubo, *Microporous and Mesoporous Mater.*, 2017, **245**, 1-7.
- [3] R. Khare, D. Millar and A. Bhan, *J. Catal.*, 2015, **321**, 23-31.
- [4] C. Y. Lee, Y.-S. Bae, N. C. Jeong, O. K. Farha, A. A. Sarjeant, C. L. Stern, P. Nickias, R. Q. Snurr, J. T. Hupp and S. T. Nguyen, *J. Am. Chem. Soc.*, 2011, **133**, 5228-5231.
- [5] J. Y. Yin, X. Q. Lu, J. Y. Yan, F. Z. Su, S. Streiff, H. Xu and P. Wu, *Microporous and Mesoporous Mater.*, 2020, **305**, 110321.
- [6] J. Z. Tan, D. T. Bregante, C. Torres, D. W. Flaherty, *J. Catal.*, 2022, **405**, 91-104.